The Journal of Experimental Biology 200, 1515–1526 (1997)
Printed in Great Britain © The Company of Biologists Limited 1997
JEB0824

WAVELENGTHS OF BIOCONVECTION PATTERNS

M. A. BEES* AND N. A. HILL
Department of Applied Mathematical Studies, University of Leeds, Leeds LS2 9JT, UK

Accepted 17 March 1997

Summary

Bioconvection occurs as the result of the collective behaviour of many micro-organisms swimming in a fluid and is realised as patterns similar to those of thermal convection which occur when a layer of water is heated from below. A methodology is developed to record the bioconvection patterns that are formed by aqueous cultures of the single-celled alga *Chlamydomonas nivalis*. The analysis that is used to quantify the patterns as a function of cell concentration, suspension depth and time is described and experimental results are presented.

Key words: *Chlamydomonas nivalis*, bioconvection patterns, wavelengths, Fourier transforms, swimming micro-organisms.

Introduction

Many swimming micro-organisms are bottom-heavy and so, although their swimming directions are fairly random, they naturally tend to swim upwards (negative gravitaxis or geotaxis). Such creatures tend to aggregate at the upper boundaries of the fluid and, in sufficiently shallow layers and at low concentrations, may form a horizontally uniform, top-heavy equilibrium distribution in which the flux of cells due to upswimming is balanced by diffusion down cell concentration gradients, due to a degree of randomness in their swimming behaviour. If the micro-organisms have a higher density than the ambient fluid, then aggregations of the cells at the upper surface can initiate an overturning instability, reminiscent of thermal or Rayleigh–Bénard convection, and thus produce spatial concentration patterns. The bulk motion of the fluid exerts viscous (or frictional) torques on the micro-organisms and the resulting balance with the gravitational torque is called gyrotaxis (Kessler, 1984*b*, 1985*a*,*b*). The micro-organisms' geometry and mass distribution imply that a component of their swimming velocity is towards regions of downwelling fluid and away from upwelling fluid. In this way, the micro-organisms increase the average density of downwelling regions of fluid and cause them to sink faster. This second 'gyrotactic' instability mechanism, together with the overturning instability, drives complex patterns in suspensions of the micro-organisms which are termed bioconvection. When viewed from above, the patterns are characterized by highly concentrated aggregations of cells in both one- and two-dimensional structures. Childress *et al.* (1975) modelled bioconvection for upswimming cells in the absence of gyrotaxis and used the model to predict the wavelengths of the initial instabilities. Their analysis predicted large pattern wavelengths limited only by the size of the experimental apparatus. At any point in space, a population of micro-organisms has a random distribution of possible swimming directions, characterized by an average swimming direction and a direction- and flow-dependent diffusivity tensor (Pedley and Kessler, 1990). A deterministic model for gyrotactic bioconvection using a constant diffusivity was first analysed in layers of infinite and finite depth by Pedley *et al.* (1988) and Hill *et al.* (1989), respectively, and more realistic wavelengths were predicted. This model was further extended in a completely self-consistent fashion by Pedley and Kessler (1990) and Bees (1996), who modelled bioconvection using a probability distribution function for the cell swimming direction in a stochastic formulation of gyrotaxis. In all these works, it was found that the gyrotactic instability mechanism depends on the absolute cell concentration, unlike the overturning instability which depends on the gradient of the cell concentration.

The purpose of the present investigation is to attempt to quantify observations of pattern formation by swimming micro-organisms in a rational and reproducible manner in order to compare them with the predictions made from mathematical models of bioconvection (see Pedley and Kessler, 1990; Bees, 1996; M. A. Bees and N. A. Hill, in preparation). Observations of pattern formation have been recorded previously by such authors as Wager (1911), Loeffer and Mefferd (1952), Wille and Ehret (1968), Levandowsky *et al.* (1975) and Kessler (1984*b*), but the results have tended to be of a qualitative nature. The present study reports one of the first, controlled experiments aimed at quantitatively cataloguing aspects of the bioconvection patterns. Methods will be described that we have developed for measuring the attributes of these patterns in suspensions of a particular micro-organism, the alga *Chlamydomonas nivalis*. Fourier analysis is used to extract the dominant unstable wavenumber from the patterns as a function

*e-mail: amt5mab@amsta.leeds.ac.uk.

of time, cell concentration and suspension depth. It will be shown that this wavenumber increases with time, not continuously, but discretely as new modes become unstable on top of already developed modes. Observations of pattern development and mode interactions will be discussed.

Materials and methods

Homogeneous cultures of fully motile *Chlamydomonas nivalis* (Wille) cells were cultured in Bold's Basal Medium to which vitamin B12 ($1\,\mu g\,l^{-1}$) was added to encourage motility (Bold and Wynne, 1978; James, 1978). Subcultures were taken every 6 weeks and left under two, cool-white fluorescent tube lights which gave a maximum light intensity of 500 lx with a 12 h:12 h L:D photoperiod. There is some evidence to suggest (J. O. Kessler, personal communication) that the cells are not gyrotactic within the first week after subculturing, so experiments were conducted on approximately 4-week-old cultures, at a predetermined time in the middle of the day when the cells are most active (Tomson and Demets, 1989). All steps of the breeding and experimental processes took place at a constant temperature (25±2 °C) within the laboratory. All the equipment required for culturing was washed and rinsed in distilled water and then carefully sterilized (autoclaved at a pressure of 100 kPa for 15 min) to avoid contamination by bacteria and fungi. *C. nivalis* are negatively gravitactic and thus are easy to concentrate above a plug of absorbent cotton wool placed in the neck of a flask 1 cm below the surface of the suspension (Kessler, 1982, 1984*a*). The concentrated suspension can be transferred by pipette to a Petri dish. It was found that plastic Petri dishes were the most regularly shaped (maximum variation in depth approximately 0.03 mm) and the 5 cm diameter, circular, sterile variety was generally used. One of the first reactions of the cells when the suspension is put into the Petri dish is to stick to the surfaces of the dish. To avoid this problem, a small amount of clear medium from the culture flask was put into the Petri dish before the dish was cleaned and polished with a lens tissue. If the cells still stuck following this procedure, then the dish and suspension were left in darkness for 24 h. This usually gave the cells sufficient time to adapt, and thereafter reproducible patterns were generally observed.

As well as being gravitactic and gyrotactic, *C. nivalis* are phototactic (Foster and Smyth, 1980). The cells also exhibit a photophobic response to a sharp increase in light intensity: they stop swimming for a short period before eventually adjusting their swimming stroke, such that their flagella are both aligned, and swimming in the reverse direction (Witman, 1993; Rüffer and Nultsch, 1985). Therefore, a very low intensity, red light source at wavelengths of approximately 622–780 nm, to which *C. nivalis* do not respond significantly, was used to illuminate them (Foster and Smyth, 1980). An infrared filter was placed between the light source and the cells, and a milk glass filter was used directly under the suspension to create an even, non-directional light source. The light intensity at the final stage did not exceed 5 lx, measured using a standard light meter.

Mean concentration measurements were conducted after the experiments were completed by first killing the cells, using iodine or by heating them, and then sampling from the well-mixed suspension using a microslide. When an end of the microslide is placed in the suspension, fluid and cells are drawn into it by capillary action. Tests were conducted to ensure that this method produced a representative sample. The microslides are hollow tubes of rectangular cross section, 0.2 mm by approximately 1 mm by 40 mm (depth × width × length) and thus the volume per unit area, when the slide is flat on a table, is easily calculated. When the cells are dead, they sink to the bottom of the slide. Using a Leitz stereo microscope linked to a Z80-based Seescan (Cambridge) image-processing system, the number of cells in the picture was counted automatically and, after calibration using a graticule and manual counts, the cell concentration was calculated. The microscope was arranged with a light source directly below the microslide. The light was adjusted so that it was focused through the spheroidal cells onto the video lens, producing pinpoints of bright light in the centres of the cells and thus allowing touching cells to be counted independently. To measure the depth of the suspensions, a calibrated microscope was used that was first focused on the bottom of the Petri dish and then on the surface of the suspension. The microscope was calibrated using glass slides of known thickness (measured using a micrometer). Depths could be measured to within ±0.03 mm.

A video camera was connected directly to the image processor to capture images of the bioconvection patterns which were then analysed on a Unix-based workstation. In general, the suspensions were mixed well, and then pictures were captured every 10 s. Careful, uniform mixing with little swirling is very important since, if the initial fluid motion is too vigorous, it takes a sufficiently long time to decay that it significantly influences the pattern formation (see Discussion). Small-amplitude manual oscillations were found to be best for this purpose. For each of the experiments, nine pictures were captured and saved on magnetic disks, and these pictures were then transferred *via* a PC 286 to the Unix system. The wavelengths of the patterns in the images were calculated using two-dimensional Fourier transforms generated using an image-processing software package, IDL (Research Systems Inc., Colorado, USA), on the workstation.

The images consist of 256 pixels × 256 pixels of 128 grey shades. The sets of nine pictures each contain unwanted information such as the walls of the dish, reflections and scratches on the dish, localized or irregular light sources, and the boundary of the picture. The first three of these can be eliminated by subtracting the first image, when there is no bioconvection, from the next eight images. However, the boundary of the picture becomes important when analysing the images using Fourier methods. Suitable use of windowing functions can solve this problem. The two-dimensional Fourier transform of an image contains all of the information that existed in the original image but expressed in terms of the

amplitude, phase and direction of its sinusoidal components. The Fourier spectrum (or power spectrum) is calculated in order to provide the sum of the amplitudes of the spectral components at a particular wavelength in any direction or phase. Thus, by Fourier-transforming the images and obtaining their Fourier spectra, it is possible to extract a measure of the dominant wavelength at a given instance and to investigate how it changes with time.

We define the wavenumber as the number of complete sinusoidal waves contained in a length of the same size as the image's width. Hence, the wavenumber, k, is related to the physical wavelength, λ, by:

$$k = \frac{I_w}{\lambda} \ , \tag{1}$$

where I_w is the image width and equals 5.2 cm in our experiments. We transform the physical image space to a space consisting of wavenumbers by using the Fourier transform. The original image consists of a finite number of discrete pixels, and so we use the Fast Fourier Transform (FFT) algorithm developed by Cooley and Tukey (1965) (see Bingham, 1974, for a history of the method) to construct the discrete Fourier transform of the images. The FFT is an efficient algorithm for constructing discrete Fourier transforms that avoids repeating identical algebraic operations. Press *et al.* (1992) describe the workings of the FFT succinctly. The discrete Fourier transform, $H(k_x, k_y)$, of an image, $h(x, y)$, of size N^2 in two dimensions is given by:

$$H(k_x, k_y) = \sum_{y=0}^{N-1} \sum_{x=0}^{N-1} \exp\left(\frac{2\pi i k_x x}{N}\right) \exp\left(\frac{2\pi i k_y y}{N}\right) h(x, y) \ , \tag{2}$$

where k_x and k_y are wavenumbers in the x and y directions, respectively, and $i=\sqrt{-1}$. $H(k_x, k_y)$ is, in general, a complex two-dimensional array and contains phase and wavenumber information. A procedure in the graphics package IDL was used to perform the FFT on the real, two-dimensional image array. The procedure returns a complex array of the same size. The number of pixels in the image, N=256, is sufficient to resolve bioconvection structures in the pictures (and thus satisfy the Nyquist condition of at least two pixels per waveform).

The Fourier spectrum is a measure of the spectral components of an image at varying wavenumbers, irrespective of their direction, and so is a useful tool for highlighting the dominant wavenumbers contained in the image. The discrete Fourier spectrum, P_n, is defined on $N/2$ intervals (called bins), $I_n=(n, n+1)$ where n=0,...., (N/2)−1, as:

$$P_n = \sum_{d(k_x, k_y) \in I_n} |H(k_x, k_y)|^2 \tag{3}$$

where $d(k_x, k_y)=\sqrt{(k_x^2+k_y^2)}$ is the distance in Fourier space of (k_x, k_y) from the origin. If the scales in h space for x and y are different (depending on the construction of the video camera), then it will be necessary to scale the distance (i.e. either k_x or k_y) in the transform space, H, accordingly. We shall discuss what we can do with the Fourier spectrum after describing potential sources of error.

As the two-dimensional FFT is essentially two FFTs performed in the x and y directions consecutively, we may consider the errors from the discretisation separately in each direction. The image has an edge and, hence, we are in effect multiplying the original infinite image by a square 'windowing function' prior to calculating its Fourier transform. This is equivalent to finding the convolution of the image Fourier space with that of the square-window Fourier space. Hence, there is a certain amount of 'leakage' from one bin to the next due to the windowing function, and it can be shown that it has a typical fall-off rate of $(\pi\tilde{k})^{-2}$, where $\tilde{k}$ is the wavenumber offset in bins (Press *et al.* 1992, pp. 545–551). Leakage can cause many types of error, the most obvious yet least destructive of which is a loss of detail due to smoothing. The square of the transformation of the window function determines the leakage, Λ, where:

$$\Lambda(\tilde{k}) = \frac{1}{W_{ss}} \left| \sum_{x=0}^{N-1} \exp\left(\frac{2\pi i \tilde{k} x}{N}\right) W(x) \right|^2 \ , \tag{4}$$

where $W(x)$ is the windowing function and

$$W_{ss} = N \sum_{x=0}^{N-1} W^2(x) \ .$$

For a square windowing function,

$$\Lambda(\tilde{k}) = \frac{1}{N^2} \left\{ \frac{\sin\pi\tilde{k}}{\sin[(\pi\tilde{k})/N]} \right\}^2 \ . \tag{5}$$

For Fourier spectrum analyses, it is the oscillatory nature of the leakage which is undesirable (a manifestation of the Gibbs phenomenon whereby sharp edges introduce oscillatory errors). A solution is to use a different windowing function that does not have the sharp edges of the square windowing function. The Hann window was chosen (Press *et al.* 1992, pp. 545–549) as it removes the oscillatory nature of the leakage and the error rapidly decreases to zero with $|\tilde{k}|$. The Hann window is essentially a cosine (plus a constant) about the centre of the image and reaches a minimum of zero at the edges. This has the additional benefit of favourably weighting the information in the centre of the picture. The Hann window in two dimensions is defined as:

$$W_H(x, y) = \frac{1}{4}\left(1 - \cos\frac{2\pi x}{N}\right)\left(1 - \cos\frac{2\pi y}{N}\right) \tag{6}$$

and is multiplied with the image before application of the FFT algorithm.

In general, the discrete Fourier spectra that were found in these experiments can be plotted as rather noisy bar charts with one or more dominant wavenumbers (see Fig. 1). An

unnormalised double Gaussian distribution was chosen to fit the spectra where the first Gaussian is fitted to the dominant, most unstable wavenumber and the second is fitted to the remainder, which consists of 'noise' and the lesser modes. The unnormalised double Gaussian distribution, $\bar{\Gamma}(X=n)$, is defined as:

$$\bar{\Gamma}(X=n) = A_1 \exp\left[-\left(\frac{x+\mu_1}{\lambda_1}\right)^2\right] + A_2 \exp\left[-\left(\frac{x+\mu_2}{\lambda_2}\right)^2\right], \quad (7)$$

where A_1, A_2, μ_1, μ_2, λ_1 and λ_2 are constants fitted to the data using the least-squares algorithm. Fig. 1 shows an example of this curve fitting. μ_1 provides a measurement of the wavenumber of the dominant pattern contained in the image. It was found that this method proved successful unless two or more large peaks were present, in which case the dominant modes were estimated manually.

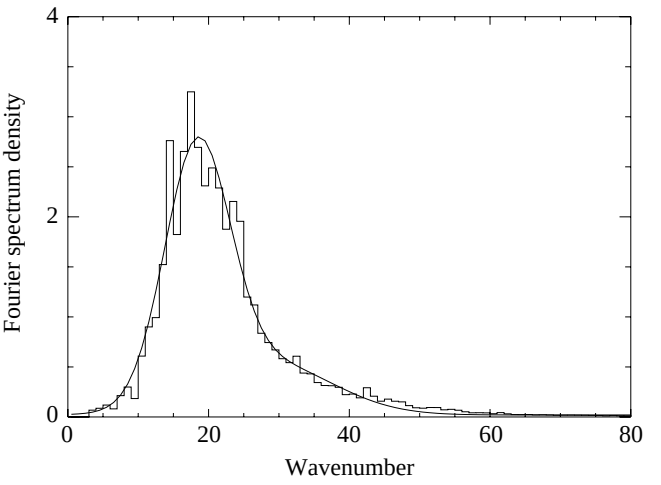

Fig. 1. An example of curve fitting using the unnormalised double Gaussian distribution to an image's Fourier spectrum. See text for further details.

Results

The results of 39 experiments are summarised in Table 1. Three examples of bioconvection patterns are shown in Figs 2–4. Additional images can be found in Bees (1996). Dark regions indicate a high local cell concentration. Nine frames are shown for each experiment, the first eight being taken at regular intervals. The last image shown in each experiment was recorded after a sufficiently long time such that the pattern appeared steady (typically 5–10 min). Experiments were discarded if a long-term pattern did not emerge. In some such cases, it was found that the cells had begun to stick to the walls of the dish. It was assumed that the cells were separated during mixing and were able to swim to the upper surface, whereupon they promptly stuck back together and sank. This is a natural part of the cells' life cycle, in which they vary their agglutinability during the day in order to mate (Tomson and Demets, 1989), but is not relevant to the present study.

The wavenumber, k, is related to the physical wavelength, λ, by equation 1. Fig. 5 describes how the first observation (for t=20–30 s) of the most unstable (dominant) wavelength varies with cell concentration and suspension depth. In general, the wavelength increases with suspension depth and tends to decrease slightly with increasing concentration. The initial patterns observed (i.e. those 20–30 s after mixing) can be divided qualitatively into four groups: lines (L), dots (D), regular patterns of dots joined by lines in X or Y shapes and more disordered patterns of mixed modes (M). Fig. 6 shows how the pattern type varies with cell concentration and suspension depth. Lines can be seen in picture 4 (i.e. 30 s after mixing) of Fig. 2 and these are indicative of a two-dimensional instability. Dots were also observed in some experiments (e.g. picture 4 of Fig. 3), and these are formed *via* a three-dimensional instability. The more disordered or mixed pattern can be seen in Fig. 4, in which many unstable modes are present. The mixed-mode points (M in Fig. 6) indicate acute sensitivity to the initial conditions. However carefully the suspension is mixed, some residual coherent fluid motion always remains. Depending on the nature of this motion, the initial pattern will develop either as dots or as lines. In terms of the Fourier spectrum, this results in a range of equally unstable wavelengths and, depending on the initial conditions, any can dominate the pattern. However, the long-term pattern appears to be free of any such degeneracy.

The wavelength analysis was also performed on the long-term patterns and the results are given in Fig. 7. The results differ from those of the initial disturbance: the wavelength decreases with increasing cell concentration and there is no clear variation with suspension depth. The long-term pattern is independent of the initial conditions, and Fig. 7 shows much less local variation than Fig. 5. Clear differences could be seen in the shape of the Fourier spectra of the initial and long-term patterns. The initial spectra contained harmonics of the principal wavenumber and competing, unstable wavenumbers, whereas the long-term spectra contained just one unstable wavenumber and the patterns were generally characterised by regular arrays of dots (in either square or hexagonal lattices). This can be seen clearly in Fig. 4, in which it is also obvious that the pattern wavenumber increases with time. Irregular long-term patterns (e.g. Fig. 3) are hard to interpret but, the Fourier spectra suggest that they are time-dependent mode interactions of two or more modes. Other transitional types of pattern are also observed, such as the tori (labelled T in Fig. 6) seen in Fig. 3.

The wavenumber, k, usually increases from the initial instability to the final steady state (see Table 1), although it does not always do so monotonically. Fig. 8 shows results from three identical experiments performed consecutively within 10 min of each other in a region of parameter space where the patterns were sensitive to the initial conditions. It was observed that the initial instability was dependent on the type of mixing that was used even though care was taken not to set up any bulk fluid motion and whatever motion was

Table 1. *Table of experimental measurements where the subscript 0 means the first unstable mode to be measured (generally 20–30 s after mixing) and ∞ means the final pattern mode*

Expt no.	Cell concentration (cm^{-3})	Suspension depth (cm)	k_0 per dish	k_∞ per dish	λ_0 (cm)	λ_∞ (cm)	Notes
1	2.75×10^6	0.333	14.09	NA	0.369	NA	
2	2.07×10^6	0.396	10.71	NA	0.486	NA	
3	6.31×10^6	0.365	19.47	22.57	0.267	0.230	
4	3.06×10^6	0.444	11.10	17.30	0.468	0.301	
5	0.808×10^6	0.522	10.80	NA	0.481	NA	Mixed modes
6	1.02×10^6	0.729	7.50	NA	0.693	NA	Mixed modes
7	0.886×10^6	0.399	12.48	NA	0.417	NA	Mixed modes
8	1.64×10^6	0.381	15.76	NA	0.330	NA	Slow to develop
9	2.30×10^6	0.456	15.10	NA	0.344	NA	Slow to develop
10	1.88×10^6	0.690	10.00	NA	0.520	NA	Slow to develop
11	2.81×10^6	0.282	15.40	NA	0.338	NA	Mixed modes
12	2.47×10^6	0.528	8.87	19.10	0.586	0.272	Two mixed modes, starts in centre
13	2.15×10^6	0.645	10.08	18.61	0.516	0.279	Mixed modes, starts in centre
14	1.89×10^6	0.384	14.96	16.73	0.348	0.311	Images recorded every 30s
15	1.89×10^6	0.318	14.20	10.64	0.366	0.489	Images recorded every 20 s
16	3.62×10^6	0.310	17.15	14.54	0.303	0.358	
17	1.89×10^6	0.469	7.34	17.18	0.708	0.303	Two peaks, left dominant
18	1.89×10^6	0.469	14.70	14.79	0.354	0.352	Two peaks, left dominant
19	1.89×10^6	0.469	8.63	15.62	0.603	0.333	Two peaks, right dominant
20	1.89×10^6	0.723	9.97	15.11	0.522	0.344	
21	1.89×10^6	0.384	15.12	15.67	0.344	0.332	
22	2.09×10^6	0.355	14.25	16.66	0.365	0.312	
23	4.19×10^6	0.468	13.87	22.20	0.375	0.234	
24	4.19×10^6	0.291	17.26	20.62	0.301	0.252	
25	4.19×10^6	0.186	27.67	17.48	0.188	0.297	
26	4.30×10^6	0.282	19.66	22.52	0.264	0.231	
27	4.30×10^6	0.282	17.76	21.89	0.293	0.238	
28	4.30×10^6	0.282	15.75	24.19	0.330	0.215	
29	4.30×10^6	0.282	17.45	23.52	0.298	0.221	Images recorded every 20 s
30	11.8×10^6	0.342	18.08	36.84	0.288	0.141	
31	4.00×10^6	0.297	16.71	28.03	0.311	0.186	
32	15.0×10^6	0.195	28.24	28.02	0.184	0.186	
33	11.8×10^6	0.118	34.84	32.95	0.149	0.158	
34	11.8×10^6	0.168	30.59	32.72	0.170	0.159	
35	3.60×10^6	0.324	15.71	17.30	0.331	0.301	
36	11.8×10^6	0.342	15.70	25.58	0.331	0.203	
37	4.30×10^6	0.228	23.09	34.15	0.225	0.152	
38	12.2×10^6	0.300	28.73	45.19	0.181	0.115	
39	12.2×10^6	0.300	29.86	43.05	0.174	0.121	Images recorded every 30 s

Wavenumbers (normalised to the width of the Petri dish) are indicated by k and the dimensional wavelengths by λ.
NA indicates that the images were not recorded.
One image was recorded every 10 s unless stated otherwise.

present died away in under a couple of seconds. Whatever the initial instability, the patterns evolved towards the same long-term state.

Fig. 9 shows a typical example of how a pattern's Fourier spectrum evolves with time. One observation to be made concerns the oscillatory nature of the amplitude of the Fourier spectrum. The initial instability increases rapidly in amplitude until it reaches the bottom of the dish and the cells then have to swim back up to the surface. During this period, the amplitude of the unstable mode decreases. Any new instability that occurs must exist in addition to the recently set up fluid motion and, in this respect, the patterns that occur have a discrete set of wavenumbers. The overall amplitude of the Fourier spectrum thus increases when this new instability occurs. It can be seen clearly that the initial instability is composed of a set of distinct competing wavenumbers and that, as time progresses, larger and larger wavenumbers become unstable. This can be observed in Fig. 9, in which the instability peaks are indicated by a set of dark, vertical lines with constant wavenumber.

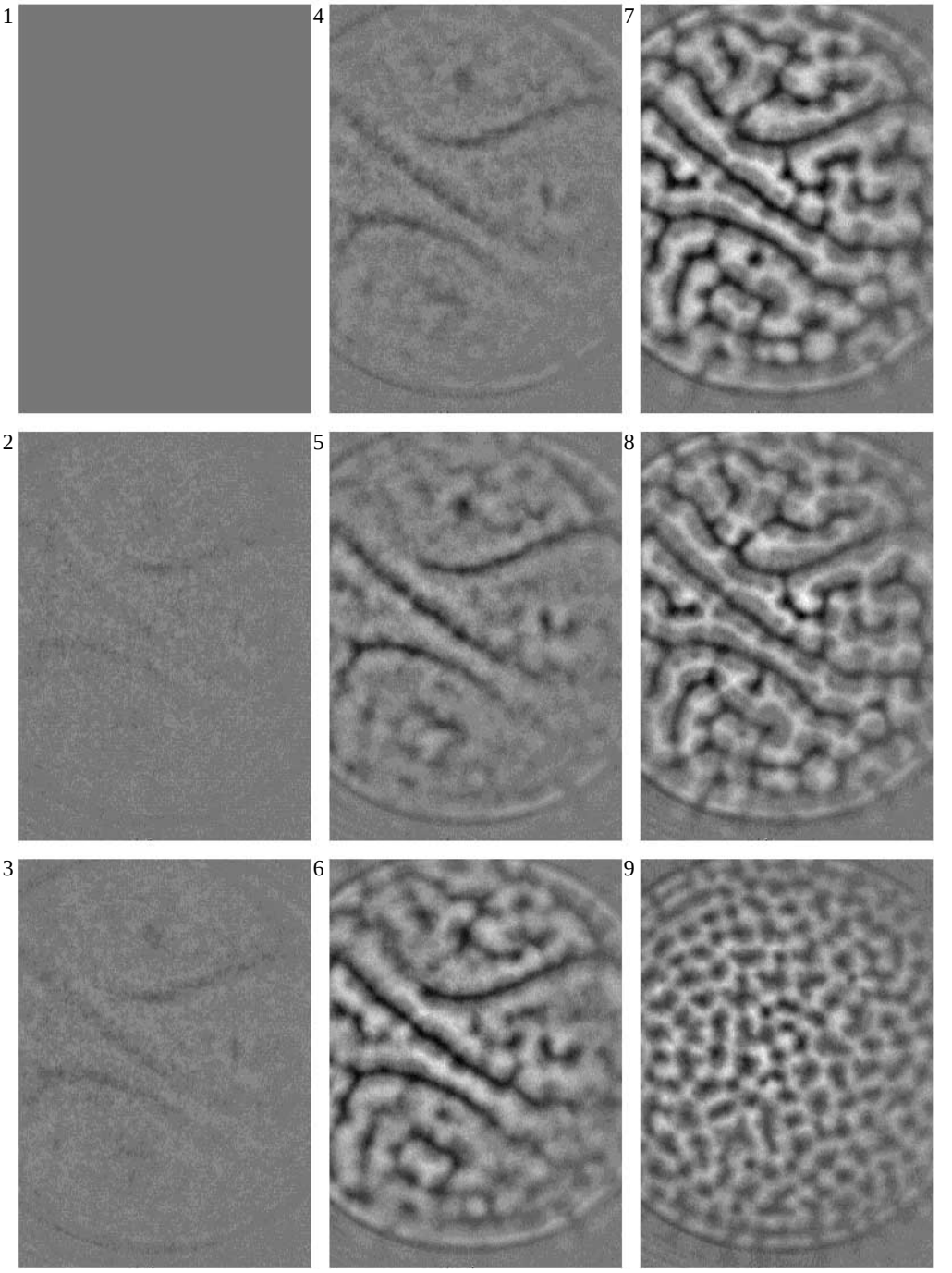

Fig. 2. Biconvection in a suspension of *Chlamydomonas nivalis* of concentration 1.89×10^6 cells cm^{-1} and depth 4.69 mm. Experiment 19 (see Table 1). Images were recorded every 10 s and are numbered in the sequence in which they were taken. Image 9 was recorded after 5 min. Dark regions indicate a high local cell concentration. Roll patterns are seen to transform into dot patterns (see text for further details).

Discussion

Initially, the suspension was agitated until it appeared to be well-mixed. To establish whether the fluid flow caused by the initial mixing had indeed diminished, we used an argument similar to that presented by Hill *et al.* (1989) and Pedley *et al.* (1988). If we assume that the Petri dish and suspension are in solid body rotation with angular velocity Ω until the container is instantaneously brought to rest (as in Hill *et al.* 1989), then the time for spin-down of the suspension is of order $E^{1/2}\Omega^{-1}$ s, where E is the Ekman number. Hill *et al.* (1989) show that if Ω approximates $1\,s^{-1}$ then the decay time is approximately 10 s. This is larger than the upper estimate of Pedley *et al.* (1988) of a decay time of 5 s when the typical stirring velocity is $0.1\,cm\,s^{-1}$. A value of 10 s is sufficient for the initial bioconvection patterns to be independent of the mixing (e.g. Figs 3, 4). However, the patterns formed in certain regions of parameter space were acutely sensitive to the form of mixing used (see Figs 2, 8), as shown by Fig. 6 in which many pattern types occupy the same region in parameter space.

One of the objectives of these experiments was to provide data which can be compared with future theoretical predictions from mathematical models of bioconvection. Computer simulations of bioconvection are currently being developed and are needed to predict the development of long-term

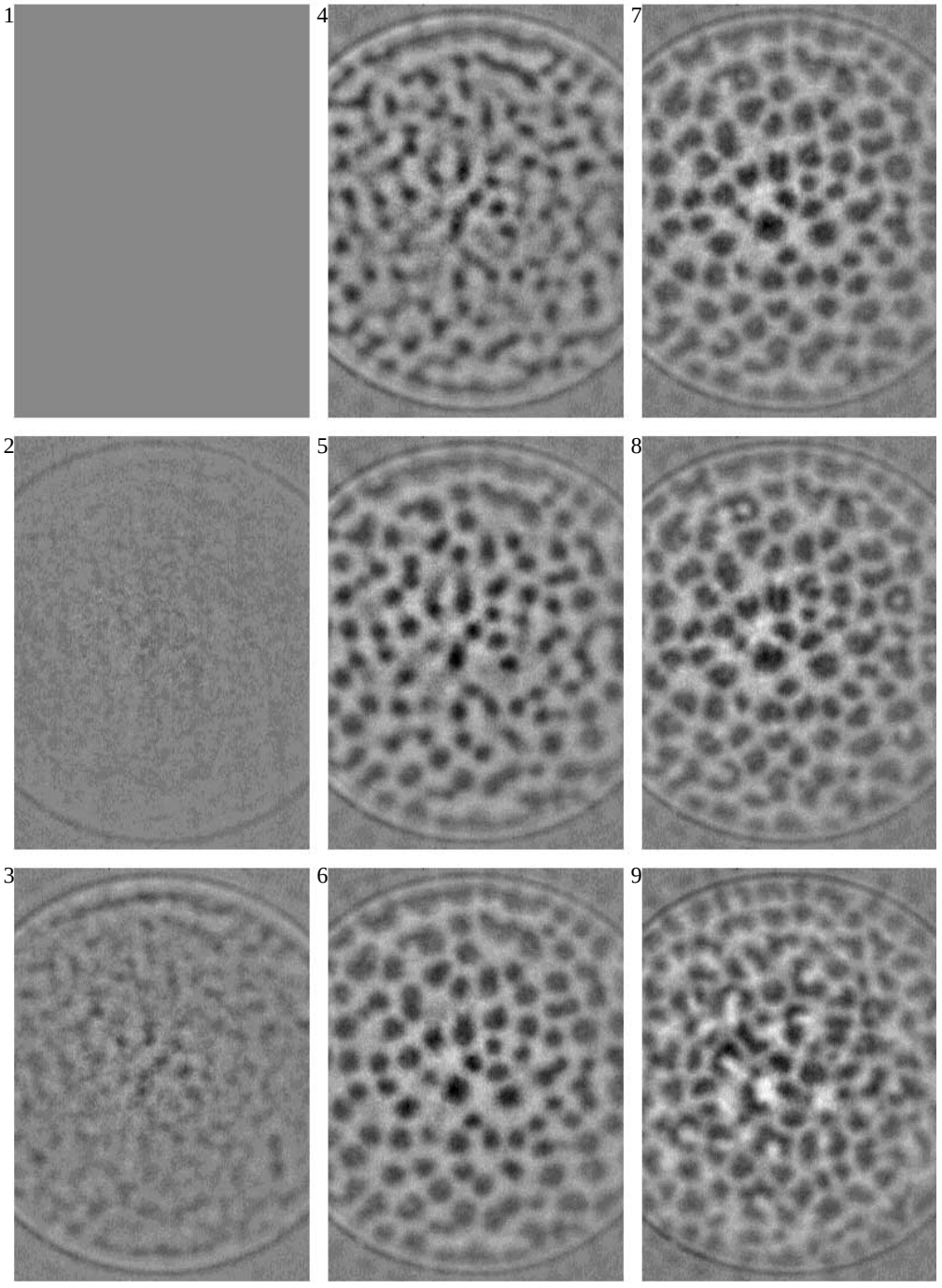

Fig. 3. Biconvection in a suspension of *C. nivalis* of concentration 1.89×10^6 cells cm^{-1} and depth 3.18 mm. Experiment 15 (see Table 1). Images were recorded every 20 s and and are numbered in the sequence in which they were taken. Image 9 was recorded after 5 min. Dark regions indicate a high local cell concentration. Annular or ring-like patterns are clearly observed in the final three frames (7–9).

patterns because they are caused by nonlinear mechanisms. So far, mathematical approaches have been limited to predictions of the onset of pattern formation using linear theory. These assume that initially there is no bulk flow of the suspension of micro-organisms and examine the effects of small perturbations on a specified initial concentration distribution of cells. It is difficult to achieve such an idealized initial state in experiments owing to the presence of residual fluid motion after mixing and the inevitable non-uniformities in cell concentration. Nevertheless, some comparisons can be made and used to determine boundaries for some of the parameters which are difficult to measure accurately. The results from seven experiments (numbers 2, 4, 7, 17, 18, 19 and 23 in Table 1) have been selected as a representative sample for these comparisons and, also, they are of approximately the same depth, 0.4 cm.

In general, an initial instability is manifest after 20–30 s, and if the cells swim at approximately 50 $\mu m\,s^{-1}$ (Pedley and Kessler, 1992; Hill and Häder, 1997), then they travel 1.0–1.5 mm in this time. Since the depth of the whole layer is of the order of 4 mm, the equilibrium distribution described above will not have had sufficient time to form fully. Thus, if the initial patterns are caused essentially by the overturning instability due to the top-heavy cell concentration profile, only

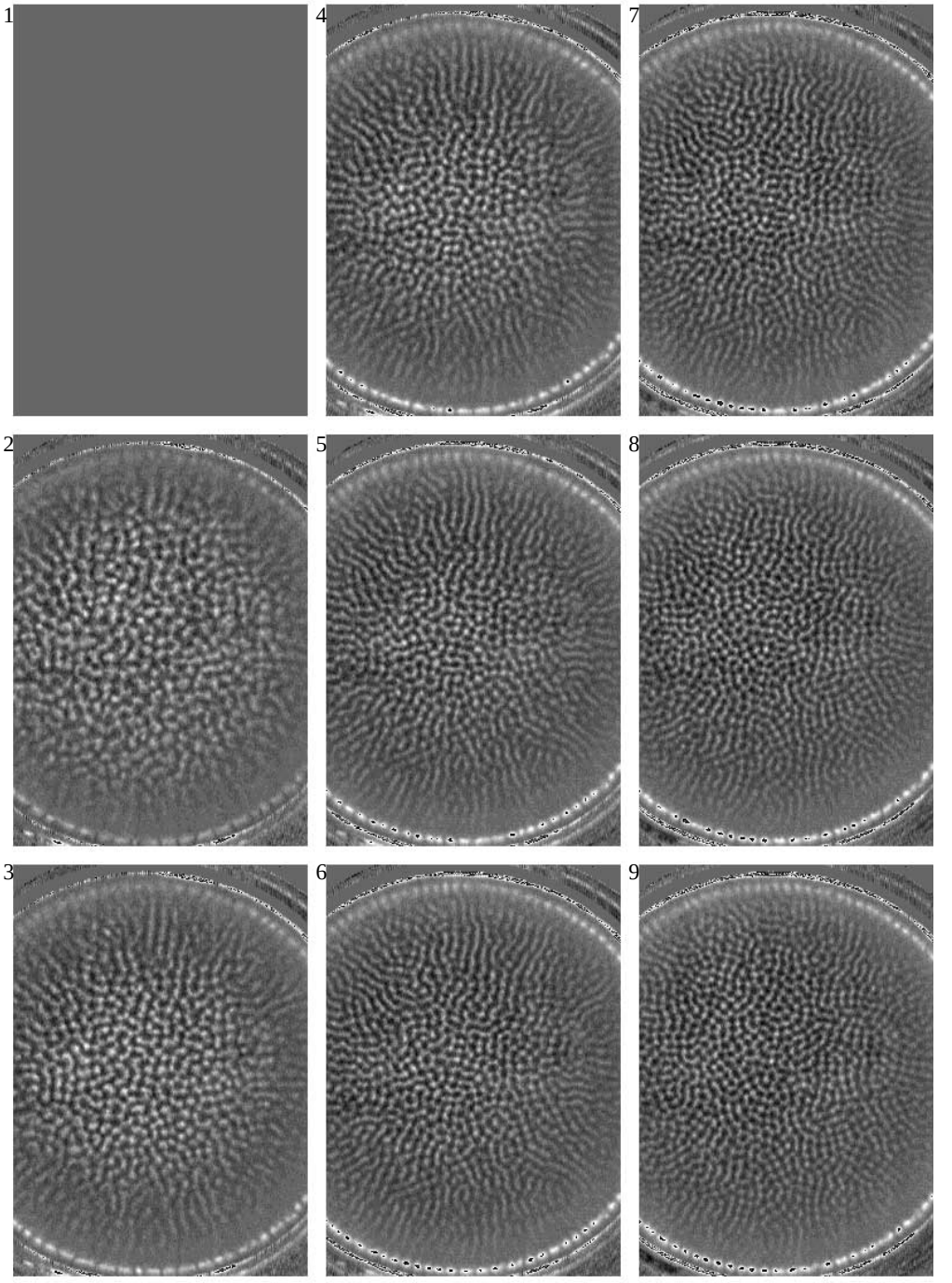

Fig. 4. Biconvection in a suspension of *C. nivalis* of concentration 12.2×10^6 cells cm^{-1} and depth 3.00 mm. Experiment 39 (see Table 1). Images were recorded every 30 s and and are numbered in the sequence in which they were taken. Dark regions indicate a high local cell concentration. Tightly packed, regular structures are observed on a variety of scales and there is some interaction between the horizontal boundaries whose influence propagates towards the centre with time.

a small proportion of the cells will be involved and the mean concentration, c, of cells must be significantly greater than the minimum, critical concentration at which the equilibrium profile becomes unstable to small perturbations. The critical cell concentration depends on a parameter, d, proportional to the depth of the layer, and is expressed in terms of a dimensionless parameter called the Rayleigh number, R, which is proportional to c and d^4. Linear theories of the initial instability predict the critical values of the Rayleigh number, R_c, and also the initial wavelengths, λ, of the bioconvection patterns. The theoretical results for the simpler mathematical model of Pedley *et al.* (1988) and Hill *et al.* (1989), in which the randomness in cell swimming direction was modelled by a constant cell swimming diffusivity, D, are based on two possible initial concentration profiles, namely the equilibrium profile in a layer of finite depth and a uniform profile suitable for the analysis of relatively deep layers. Using the analysis and parameter values chosen by Hill *et al.* (1989; see their Table 2), we can conclude that the experimental values of R (Table 2) are approximately five times greater than R_c for the equilibrium profile ($R_c^{(e)}$) and of the same order as R_c for the uniform profile ($R_c^{(u)}$). This is consistent with the experimental

Table 2. *Experimental measurements of dominant wavelengths λ_0 of the initial disturbance and corresponding calculations of* d *(proportional to suspension depth) and the Rayleigh number,* R*, depending on the value of the correlation time,* τ

Experiment number	λ_0 (cm)	τ=1.3 s		τ=5 s	
		d	*R*	*d*	*R*
2	0.486	172	185×10^6	44.7	3.25×10^6
4	0.468	193	484×10^6	50.2	8.50×10^6
7	0.417	174	82.2×10^6	45.2	1.44×10^6
17	0.708	204	393×10^6	53.07	6.90×10^6
18	0.354	204	393×10^6	53.0	6.90×10^6
19	0.603	204	393×10^6	53.0	6.90×10^6
23	0.375	204	863×10^6	53.0	15.2×10^6
Theory τ=1.3 s	0.026	174	4000×10^6	–	–
Theory τ=5.0 s	0.52	–	–	45.2	7.0×10^6

Seven experiments from Table 1 have been chosen with similar suspension depths (approximately 0.4 cm) so that they can be compared with the theoretical predictions. In all cases, the gyrotactic reorientation time, *B*, equals 1.25 s. For the theoretical predictions, we assume that the depth equals 0.4 cm (see text for further details).

observation that the patterns are seen before there is sufficient time for the equilibrium state to form. Furthermore, from the equation for $R_c^{(u)}$ in Hill *et al.* (1989), we obtain an estimate of 3×10^{-4} cm s^{-1} for a lower boundary on the value of the diffusivity, *D*. However, the predicted wavelengths for the most unstable mode are approximately twice as large as the observed wavelengths. Bees (1996) and M. A. Bees and N. A. Hill (in preparation) have analysed the linear stability of the equilibrium state in a layer of finite depth using Pedley and Kessler's (1990) more rational, stochastic theory. Two key parameters in this analysis are a correlation time, τ, which is a measure of the time scale over which a cell swims in approximately the same direction, and the gyrotactic reorientation parameter, *B*, which is the time scale for

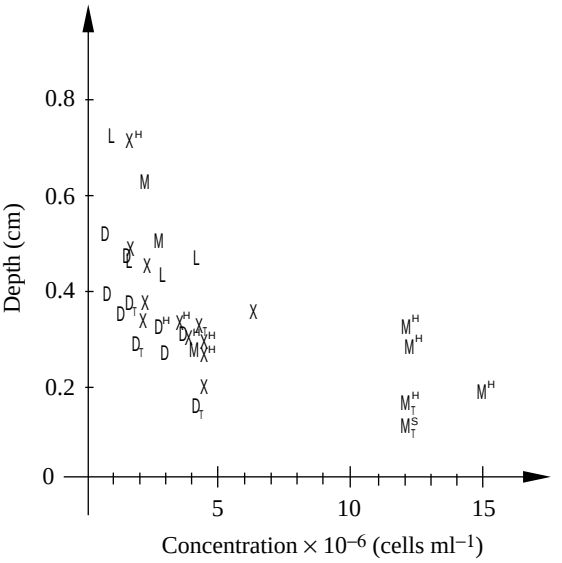

Fig. 6. Pattern type of the initial disturbance (generally 20–30 s after mixing) from a fully mixed suspension of *C. nivalis* for cell concentration and suspension depth. The dominant pattern present is shown: D, dots, L, lines, X, dots joined by lines in X or Y shapes; M, mixed. Some of the long-term patterns (the stable pattern observed after 5–10 min) are also shown: the subscript T means that the pattern evolves through a torus stage and the superscripts H and S indicate where there was clear evidence of hexagonal or square arrays, respectively, in the long-term pattern.

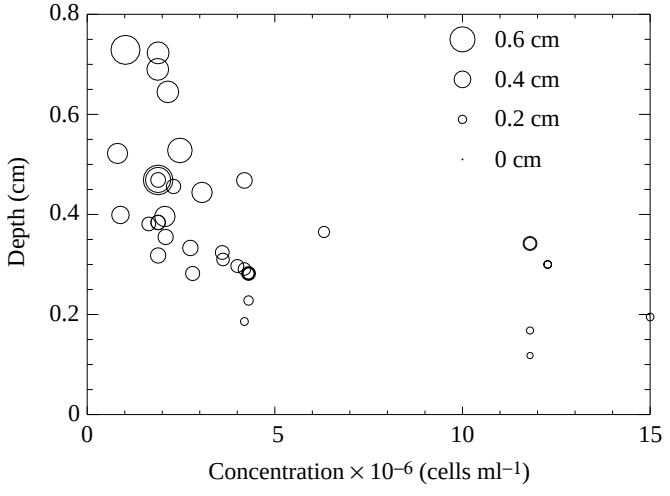

Fig. 5. Dominant wavelengths of the initial disturbance (generally 20–30 s after mixing) from a fully mixed suspension of *C. nivalis* as a function of concentration and suspension depth. The diameter of each circle represents the most unstable (dominant) wavelength. The centre of each circle represents its position in parameter space.

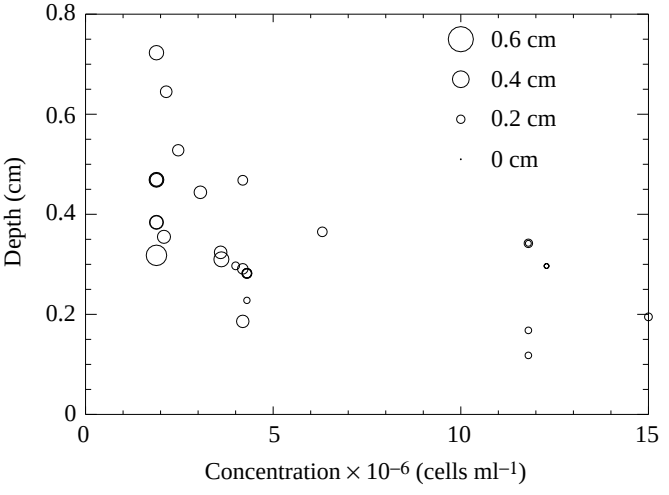

Fig. 7. Dominant wavelengths of the long-term pattern observed (5–10 min after mixing) in a suspension of *C. nivalis* as a function of cell concentration and suspension depth. The diameter of each circle represents the most unstable (dominant) wavelength. The centre of each circle represents its position in parameter space.

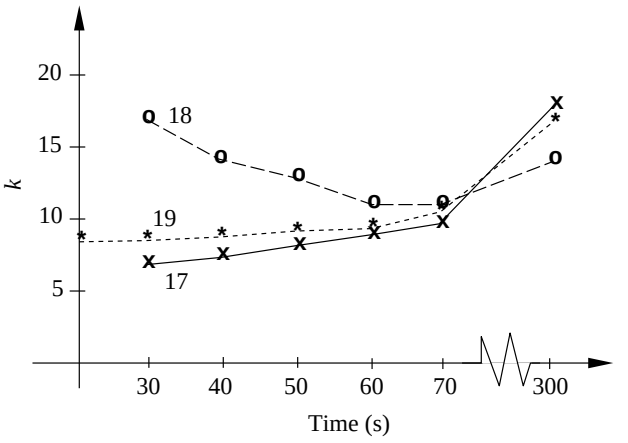

Fig. 8. Variation of the dominant pattern wavenumber k with time after mixing a suspension of *C. nivalis*. Results from three identical experiments (17–19) in which the initial instability (at t=30 s) is highly dependent on the initial conditions following mixing. The experiments were performed in the order 17, 18, 19 (see Table 1 for further details).

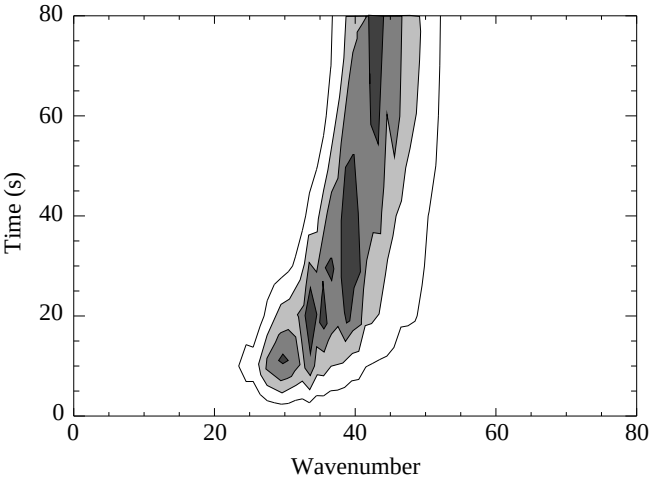

Fig. 9. A contour plot of the variation in Fourier spectrum density with time for experiment 39 (see Table 1). Different modes generally become unstable to modes of larger wavenumber. Darker regions denote higher values of Fourier spectrum density indicating a (dominant) mode with a large amplitude.

reorientation of a bottom-heavy cell in the absence of a flow. On the basis of our experience with the simpler deterministic model, we expect that, in the stochastic model, $R_c^{(e)}$ will be less than $R_c^{(u)}$ and, therefore, $R_c^{(e)}$ for the equilibrium state must still be less than the experimental values of R for which patterns are seen. This criterion shows that the estimate of τ=5 s from Pedley and Kessler (1990) gives realistic values for $R_c^{(e)}$ (see Table 2), unlike their alternative estimate of 1.3 s which gives values of $R_c^{(e)}$ one order of magnitude greater than the experimental values. Comparisons between the predicted and experimental wavelengths suggest that reasonable agreement is obtained when B≈1.25 s, a value that has been suggested from direct measurement of individual trajectories by Hill and Häder (1997).

The first instability to occur tends to consist of sheets or lines when viewed from above (although dots are also quite common). The sheet instability usually breaks down to a dot-type instability or a pattern resembling a lattice of nodes joined by lines. These patterns break down further into smaller dots or other connected patterns. Therefore, in general, two-dimensional patterns become unstable to three-dimensional patterns *via* a complicated set of mode interactions. For example, tori can be formed in the manner indicated in Fig. 10. Initially the suspension is well-mixed and the cells swim to the top, thus initiating a Rayleigh–Bénard-type instability. The initial disturbance is two-dimensional and in the form of descending sheets of concentrated suspension (bioconvection rolls). The sheets quickly break down *via* a three-dimensional instability to form descending plumes. As a plume hits the bottom of the dish, it spreads out, entraining clear fluid in its wake at the upper surface. It is when the clear fluid reaches the bottom of the dish that the resulting ring vortex can be seen clearly

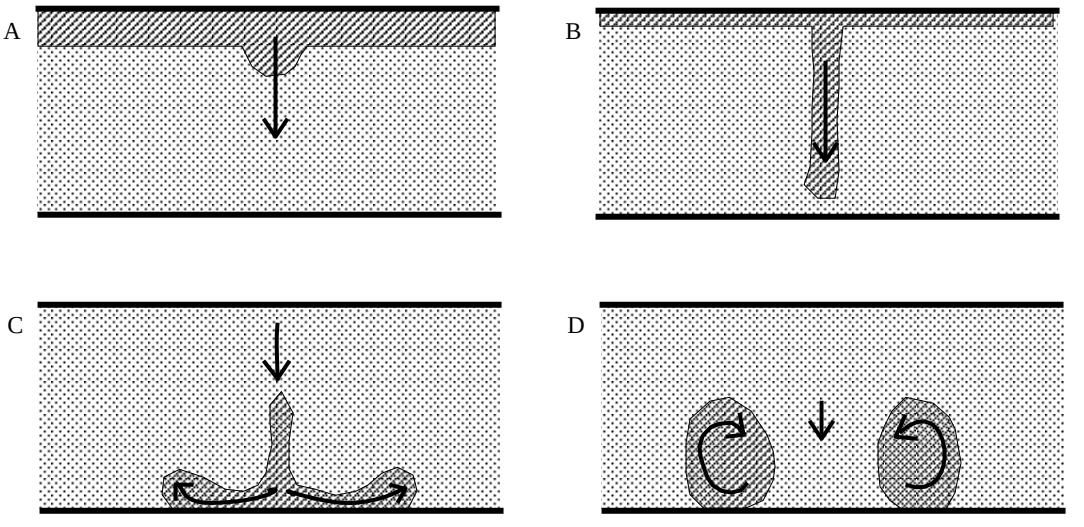

Fig. 10. Illustration to show how clear fluid can be entrained in a plume to form an annulus pattern when viewed from above. (A) Cells swim up to the top of the medium and the suspension overturns owing to a Rayleigh–Bénard instability. (B) Gyrotaxis produces thin plumes. (C) The plumes hit the bottom of the dish and spread out, forming a ring vortex. (D) Clear fluid is entrained in the wake of the plume and an annulus is created.

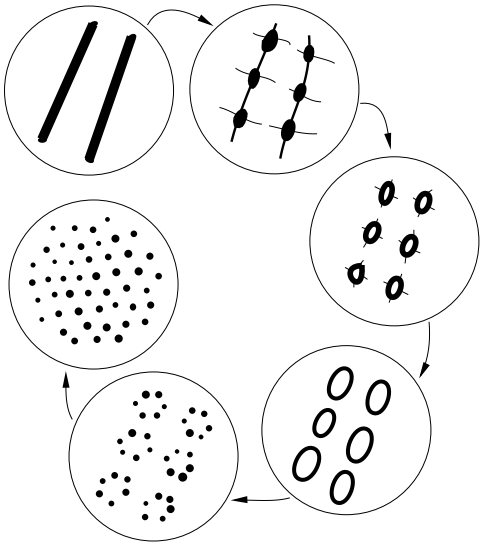

Fig. 11. Possible mode interactions viewed from above. Patterns can become unstable to other new modes. In particular, two-dimensional, rectilinear patterns can become unstable to three-dimensional dot patterns. The dot patterns can form annuli. When large enough, the annuli are essentially two-dimensional patterns and can again become unstable to three-dimensional patterns. Eventually, the pattern settles down to form a regular array of dots (e.g. see Fig. 3). In general, pattern wavelength decreases with time.

as an annulus when viewed from above. The annulus increases its diameter and forms a *closed* bioconvection roll. Eventually, this two-dimensional rotationally invariant roll becomes unstable to three-dimensional plumes (Fig. 11). This process has been observed *via* close inspection of the structures with a microscope, both from above and obliquely.

To summarize our results, we have developed techniques for recording bioconvection patterns in a shallow dish as functions of suspension concentration, depth and time. We used image-processing techniques to measure the cell concentration and suspension depth, and used methods for culturing the cells that ensured that they were always healthy and fully motile. We refined techniques for processing the images and extracting the dominant pattern wavenumber using Fourier analysis. Initial and long-term pattern wavelengths were analysed in detail and it was found that the initial wavelength increased with increasing depth but tended to decrease slightly with increasing concentration. The well-developed wavelength decreased with concentration and showed little variation with depth. When the patterns are well developed, gyrotaxis and non-linear effects become more important in regions of high local concentration and, thus, suspension depth has a less important role in determining the pattern wavenumber. Cell concentration, in contrast, does determine the final non-linear steady state (e.g. bottom-standing plumes; Pedley and Kessler, 1992). A higher cell concentration decreases the wavelength through gyrotaxis. Each of the patterns we observed was categorized, and the interaction of unstable modes as the pattern evolved with time was explored. In particular, mechanisms for the existence of annular patterns were proposed.

An additional phenomenon was observed that deserves to be reported. When the suspension was very shallow (e.g. 1.86 mm) and the cell concentration reasonably high (e.g. 4.19×10 cells cm^{-1}), then bioconvection was initiated throughout the suspension, forming dense squat plumes or 'blobs'. As time progressed, these plumes emigrated towards the edge of the dish, leaving a clear patch with no patterns. Close inspection of these plumes revealed a noticeable elevation of the upper fluid surface (sufficient to alter visibly the reflective properties of the fluid surface) directly above them, and this may have affected their stability. Concentrated plumes existed for long periods on the edge of the clear patch but tended to wander and merged with neighbours if they approached closely. It appears that these conditions may approximate the critical depth above which bioconvection can occur, and that the increase in depth at the plumes not only attracts more cells to the plumes but also decreases the depth in other regions, thus reducing the possibility of bioconvection there. The fluid layer is naturally deeper at the boundaries owing to the meniscus and, over time, this may attract more cells to the edges. We speculate additionally that a change in surface tension causes the elevation of the upper surface and also affects the attraction and merging of plumes. The excess of cells near the surface may be responsible for this change in surface tension. This phenomenon deserves further investigation.

Both authors would like to thank the Department of Biology at the University of Leeds for their help and laboratory space. M.A.B. acknowledges the financial support of an EPSRC Earmarked Studentship in Mathematical Biology.

References

BEES, M. A. (1996). Non-linear pattern generation in suspensions of swimming micro-organisms. PhD thesis, University of Leeds.

BINGHAM, E. O. (1974). *The Fast Fourier Transform*. Englewood Cliffs, NJ: Prentice-Hall.

BOLD, H. C. AND WYNNE, M. J. (1978). *Introduction to the Algae. Structure and Reproduction.* Englewood Cliffs, NJ: Prentice-Hall.

CHILDRESS, S., LEVANDOWSKY, M. AND SPIEGEL, E. A. (1975). Pattern formation in a suspension of swimming micro-organisms: equations and stability theory. *J. Fluid Mech.* **69**, 595–613.

COOLEY, J. W. AND TUKEY, J. W. (1965). An algorithm for the machine calculation of complex Fourier series. *Math. Comput*. **19**, 297–301.

FOSTER, K. W. AND SMYTH, R. D. (1980). Light antennas in phototactic algae. *Microbiol. Rev.* **44**, 572–630.

HILL, N. A. AND HÄDER, D. P. (1997). A biased random walk model for the trajectories of swimming micro-organisms. *J. theor. Biol.* (in press).

HILL, N. A., PEDLEY, T. J. AND KESSLER, J. O. (1989). Growth of bioconvection patterns in a suspension of gyrotactic micro-organisms in a layer of finite depth. *J. Fluid Mech.* **208**, 509–543.

JAMES, D. E. (1978). *Culturing Algae*. Algae Department, Carolina Biological Supply Company, Burlington, NC 27215, USA.

KESSLER, J. O. (1982). *Algal Cell Harvesting*. U.S. Patent No. 4324067.

KESSLER, J. O. (1984*a*). *Algal Cell Growth, Modification and Harvesting*. U.S. Patent No. 4438591.

KESSLER, J. O. (1984*b*). Gyrotactic buoyant convection and spontaneous pattern formation in algal cell cultures. In *Non-equilibrium Cooperative Phenomena in Physics and Related Fields* (ed. M. G. Velarde), pp. 241–248. New York: Plenum Press.

KESSLER, J. O. (1985*a*). Co-operative and concentrative phenomena of swimming micro-organisms. *Contemp. Phys*. **26**, 147–166.

KESSLER, J. O. (1985*b*). Hydrodynamic focussing of motile algal cells. *Nature* **313**, 218–220.

LEVANDOWSKY, M., CHILDRESS, W. S., SPIEGEL, E. A. AND HUTNER, S. H. (1975). A mathematical model of pattern formation by swimming microorganisms. *J. Protozool*. **22**, 296–306.

LOEFFER, J. B. AND MEFFERD, R. B. (1952). Concerning pattern formation by free-swimming microorganisms. *Am. Nat.* **86**, 325–329.

PEDLEY, T. J., HILL, N. A. AND KESSLER, J. O. (1988). The growth of bioconvection patterns in a uniform suspension of gyrotactic micro-organisms. *J. Fluid Mech.* **195**, 223–237.

PEDLEY, T. J. AND KESSLER, J. O. (1990). A new continuum model for suspensions of gyrotactic micro-organisms. *J. Fluid Mech.* **212**, 155–182.

PEDLEY, T. J. AND KESSLER, J. O. (1992). Hydrodynamic phenomena in suspensions of swimming micro-organisms. *A. Rev. Fluid Mech.* **24**, 313–358.

PRESS, W. H., TEUKOLSKY, S. A., VETTERLING, W. T. AND FLANNERY, B. P. (1992). *Numerical Recipes in FORTRAN. The Art of Scientific Computing*. Cambridge: Cambridge University Press, second edition.

RÜFFER, U. AND NULTSCH, W. (1985). High speed cinematographic analysis of the movement of *Chlamydomonas*. *Cell Motil*. **5**, 251–263.

TOMSON, A. M. AND DEMETS, R. (1989). Sexual communication in the green algae *Chlamydomonas eugametos*. PhD thesis, University of Amsterdam.

WAGER, H. (1911). The effect of gravity upon the movements and aggregation of *Euglena viridis*, Ehrb. and other micro-organisms. *Phil. Trans. R. Soc. Lond. B* **201**, 333–390.

WILLE, J. J. AND EHRET, C. F. (1968). Circadian rhythm of pattern formation in populations of a free-swimming organism, *Tetrahymena*. *J. Protozool.* **15**, 789–792.

WITMAN, G. B. (1993). *Chlamydomonas* phototaxis. *Trends Cell Biol*. **3**, 403–408.